

# Cerebral organoids model human brain development and microcephaly

Madeline A. Lancaster<sup>1</sup>, Magdalena Renner<sup>1</sup>, Carol-Anne Martin<sup>2</sup>, Daniel Wenzel<sup>1</sup>, Louise S. Bicknell<sup>2</sup>, Matthew E. Hurles<sup>3</sup>, Tessa Homfray<sup>4</sup>, Josef M. Penninger<sup>1</sup>, Andrew P. Jackson<sup>2</sup> & Juergen A. Knoblich<sup>1</sup>

The complexity of the human brain has made it difficult to study many brain disorders in model organisms, highlighting the need for an *in vitro* model of human brain development. Here we have developed a human pluripotent stem cell-derived three-dimensional organoid culture system, termed cerebral organoids, that develop various discrete, although interdependent, brain regions. These include a cerebral cortex containing progenitor populations that organize and produce mature cortical neuron subtypes. Furthermore, cerebral organoids are shown to recapitulate features of human cortical development, namely characteristic progenitor zone organization with abundant outer radial glial stem cells. Finally, we use RNA interference and patient-specific induced pluripotent stem cells to model microcephaly, a disorder that has been difficult to recapitulate in mice. We demonstrate premature neuronal differentiation in patient organoids, a defect that could help to explain the disease phenotype. Together, these data show that three-dimensional organoids can recapitulate development and disease even in this most complex human tissue.

Mammalian brain development begins with the expansion of the neuroepithelium to generate radial glial stem cells (RGs)<sup>1</sup>. These RGs divide at the apical surface within the ventricular zone (VZ) to generate neurons and intermediate progenitors. Intermediate progenitors populate the adjacent subventricular zone (SVZ), whereas neurons migrate through the intermediate zone to populate specific layers within the cortical plate. In humans, the organization of progenitor zones is markedly more elaborate; the SVZ is split by an inner fibre layer (IFL) into an inner SVZ and an outer SVZ (OSVZ)<sup>2</sup>. The OSVZ represents an entirely separate progenitor layer populated by intermediate progenitors and a unique stem cell subset termed outer radial glia (oRG)<sup>3,4</sup>, which are only present to a limited degree in rodents<sup>5</sup>. Both the IFL and OSVZ are completely absent in mice<sup>6</sup>. These key differences allow for the striking expansion in neuronal output and brain size seen in humans<sup>7,8</sup>.

Primary microcephaly is a neurodevelopmental disorder in which brain size is markedly reduced<sup>9</sup>. Autosomal-recessive mutations have been identified in several genes, all of which encode proteins localizing to the mitotic spindle apparatus<sup>10</sup>. Heretofore, primary microcephaly pathogenesis has primarily been examined in mouse models. However, mouse mutants for several of the known genes<sup>11–14</sup> have failed to recapitulate the severely reduced brain size seen in human patients.

Given the dramatic differences between mice and humans, methods that recapitulate paradigms of human brain development *in vitro* have enormous potential. Although considerable progress has been made for *in vitro* models of whole-organ development for other systems—such as intestine<sup>15</sup>, pituitary<sup>16</sup> and retina<sup>17,18</sup>—a three-dimensional culture model of the developing brain as a whole has not been established. Previous studies have modelled certain isolated neural tissues *in vitro*<sup>19–23</sup>, including dorsal cerebral cortical tissue, which could recapitulate many aspects of early development. However, later events such as the formation of discrete cortical layers with stereotypical inside-out organization as well as human characteristics, such as the presence of oRG cells and the unique organization of progenitor zones, were not described.

Here we describe a three-dimensional culture system for deriving brain tissue *in vitro*. These so-called cerebral organoids develop a variety

of regional identities organized as discrete domains capable of influencing one another. Furthermore, cerebral cortical regions display an organization similar to the developing human brain at early stages, as well as the presence of a considerable oRG population. Moreover, cerebral cortical neurons mature to form various pyramidal identities with modest spatial separation. Finally, we use patient-derived induced pluripotent stem (iPS) cells and short hairpin RNA (shRNA) in these organoids to model CDK5RAP2-dependent pathogenesis of microcephaly, a disorder that has been difficult to model in mice.

## Generation of cerebral organoids

Recent progress with *in vitro* models of various organ systems has demonstrated the enormous self-organizing capacity for pluripotent stem cells to form whole tissues<sup>15,18</sup>. We built upon this concept and developed a protocol without the use of patterning growth factors, focusing instead on improving growth conditions and providing the environment necessary for intrinsic cues to influence development. We began with a modified approach to generate neuroectoderm from embryoid bodies<sup>24</sup>. Neuroectodermal tissues were then maintained in three-dimensional culture and embedded in droplets of Matrigel to provide a scaffold for more complex tissue growth. These Matrigel droplets were then transferred to a spinning bioreactor to enhance nutrient absorption (Fig. 1a). This method led to rapid development of brain tissues, which we termed cerebral organoids, requiring only 8–10 days for the appearance of neural identity and 20–30 days for defined brain regions to form.

Cerebral organoids at early stages (15–20 days) formed large, continuous neuroepithelia surrounding a fluid-filled cavity reminiscent of a ventricle with characteristic apical localization of the neural specific N-cadherin (Fig. 1b). Furthermore, the neuroepithelium was larger and more continuous than tissues generated using a stationary approach<sup>20</sup>, which instead formed an aggregate of several small rosette-like neuroepithelia (Fig. 1b and Extended Data Fig. 1a).

Although tissues reached maximal size by 2 months, cerebral organoids formed large (up to 4 mm in diameter), complex heterogeneous

<sup>1</sup>Institute of Molecular Biotechnology of the Austrian Academy of Science (IMBA), Vienna 1030, Austria. <sup>2</sup>MRC Human Genetics Unit, Institute of Genetics and Molecular Medicine, University of Edinburgh, Edinburgh EH4 2XU, UK. <sup>3</sup>Wellcome Trust Sanger Institute, Cambridge CB10 1SA, UK. <sup>4</sup>Department of Clinical Genetics, St. George's University, London SW17 0RE, UK.

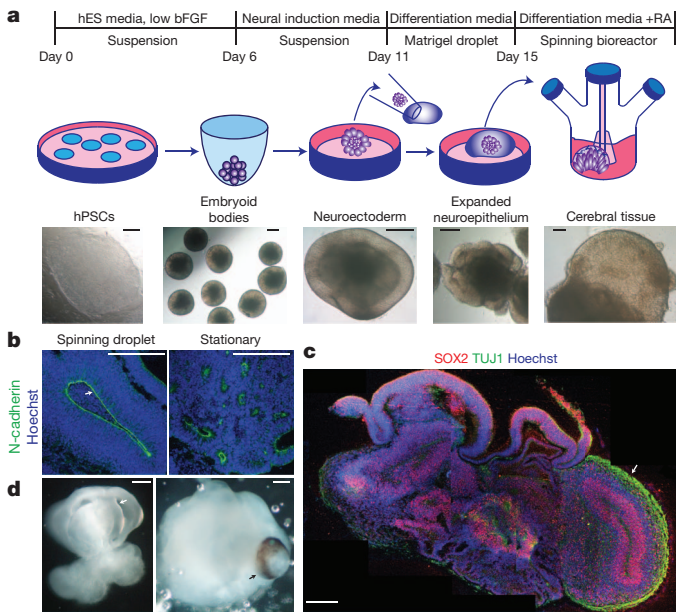


**Figure 1 | Description of cerebral organoid culture system.** **a**, Schematic of the culture system described in detail in Methods. Example images of each stage are shown. bFGF, basic fibroblast growth factor; hES, human embryonic stem cell; hPSCs, human pluripotent stem cells; RA, retinoic acid. **b**, Neuroepithelial tissues generated using this approach (left) exhibited large fluid-filled cavities and typical apical localization of the neural N-cadherin (arrow). These tissues were larger and more continuous than tissues grown in stationary suspension without Matrigel (right). **c**, Sectioning and immunohistochemistry revealed complex morphology with heterogeneous regions containing neural progenitors (SOX2, red) and neurons (TUJ1, green) (arrow). **d**, Low-magnification bright-field images revealing fluid-filled cavities reminiscent of ventricles (white arrow) and retina tissue, as indicated by retinal pigmented epithelium (black arrow). Scale bars, 200  $\mu\text{m}$ .

tissues, which could survive indefinitely (currently up to 10 months) when maintained in a spinning bioreactor. Histological and gross morphological analysis revealed regions reminiscent of cerebral cortex, choroid plexus, retina and meninges (Fig. 1c, d and Extended Data Fig. 1b). Notably, tissues typically reached a size limit, probably because of the lack of a circulatory system and limitations in oxygen and nutrient exchange. Consistent with this, extensive cell death was visible in the core of these tissues (Extended Data Fig. 1c), whereas the various brain regions developed along the exterior. Furthermore, cerebral organoids could be reproducibly generated with similar overall morphology and complexity from both human embryonic stem (ES) cells and iPS cells (Extended Data Fig. 1d, e).

### Cerebral organoids display discrete brain regions

Brain development *in vivo* exhibits a striking degree of heterogeneity and regionalization as well as interdependency of various brain regions. Histological analysis suggested that human cerebral organoids might similarly display heterogeneous brain regions. To examine this further, we first tested the efficiency of initial neural induction in these tissues by performing reverse transcriptase PCR (RT-PCR) for several markers of pluripotency and neural identity (Extended Data Fig. 2a). As expected, pluripotency markers OCT4 (also known as POU5F1) and NANOG diminished during the course of organoid differentiation, whereas neural identity markers SOX1 and PAX6 were upregulated, indicating successful neural induction.

To test for early brain regionalization in whole organoids, we performed RT-PCR for forebrain (FOXP1 and SIX3) and hindbrain (KROX20 (also known as EGR2) and ISL1) markers (Fig. 2a), revealing the presence of both populations within the tissue. However, as tissue development proceeded, forebrain markers remained highly expressed whereas hindbrain markers decreased, reminiscent of the

developmental expansion of forebrain tissue during human brain development<sup>25</sup>.

In order to test whether cells with these brain region identities developed as discrete regions within the organoids, as gross morphology would suggest, or were randomly interspersed within the tissue, we performed immunohistochemical staining for markers of forebrain, midbrain and hindbrain identities during early development of these tissues (16 days; Fig. 2b and Extended Data Fig. 2b). PAX6 expression revealed several regions of forebrain identity, and OTX1 and OTX2 expression marked forebrain/midbrain identity. These regions were located adjacent to regions that lacked these markers but that were positive for hindbrain markers GBX2, KROX20 and PAX2, which was reminiscent of the early mid-hindbrain boundary, suggesting similar regional communication and probably mutual repression.

*In vivo* brain development involves increasing refinement of regional specification. Therefore, we examined further-developed cerebral organoid tissues for regional subspecification. We performed staining for the forebrain marker FOXP1 (Fig. 2c), which labelled regions displaying typical cerebral cortical morphology. Many of these regions were also positive for EMX1 (Fig. 2d), indicating dorsal cortical identity. We also tested for further subregionalization by staining for cortical lobe markers, namely AUTS2, a marker of prefrontal cortex<sup>26</sup> (Fig. 2e); TSHZ2, a marker of the occipital lobe<sup>26</sup> (Extended Data Fig. 2c); and LMO4, a marker of frontal and occipital lobes but absent in parietal lobes<sup>26</sup> (Extended Data Fig. 2c). These markers could be seen in neurons labelling distinct regions of dorsal cortex, suggesting subspecification of cortical lobes.

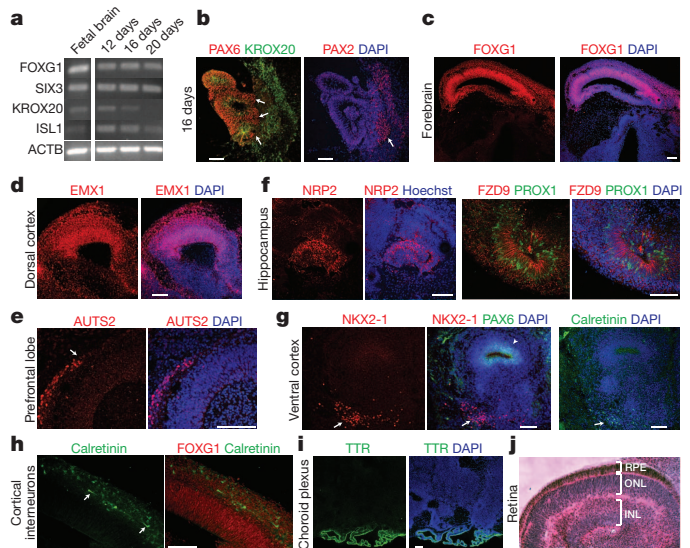


**Figure 2 | Human cerebral organoids recapitulate various brain region identities.** **a**, RT-PCR for forebrain markers (FOXP1 and SIX3) and hindbrain markers (KROX20 and ISL1) at 12, 16 and 20 days of differentiation. Human fetal brain complementary DNA was used as positive control.

**b**, Immunohistochemistry in serial sections for the forebrain marker PAX6 (red, left) and the hindbrain markers KROX20 (green, left) and PAX2 (red, right) at 16 days of differentiation. Note the juxtaposition reminiscent of the mid-hindbrain boundary (arrows). DAPI (4',6-diamidino-2-phenylindole) marks nuclei (blue). **c-i**, Staining for various brain region identities: forebrain, FOXP1 (c); dorsal cortex, EMX1 (d); prefrontal cortex (note the discrete boundary, arrow), AUTS2 (e); hippocampus, NRP2, FZD9, PROX1 (f); ventral forebrain, NKX2-1 (g) and choroid plexus, TTR (i). **g**, Staining for adjacent ventral (arrow) and dorsal (PAX6, arrowhead) forebrain and for calretinin (green) in a serial section revealing cortical interneurons in the ventral region (arrow). Calretinin interneurons within dorsal cortex (h) exhibit typical morphology of tangential migration (arrows). **j**, Haematoxylin and eosin staining of retinal tissue exhibiting stereotypical layering: retinal pigment epithelium (RPE), outer nuclear layer (ONL) and inner nuclear layer (INL). Scale bars, 100  $\mu\text{m}$ .

Furthermore, staining for markers of the hippocampus (Fig. 2f) and ventral forebrain (Fig. 2g) revealed specification of these regions, although they did not organize to form the overall structure seen *in vivo*. Notably, interneurons produced in ventral forebrain regions exhibited a morphology and location consistent with migration from ventral to dorsal tissues (Extended Data Fig. 2d). Within the dorsal cortex, these neurons displayed neurites parallel to the apical surface, reminiscent of the migratory extensions seen in tangential migration *in vivo* (Fig. 2h). Notably, calretinin<sup>+</sup> interneurons were absent from the dorsal cortex of organoids lacking a ventral region (4 out of 4 NKX2-1-negative organoids), suggesting that interneurons originate in the ventral forebrain to migrate to the dorsal cortex. This suggests that distant regions can influence one another in developing cerebral organoids.

Finally, other brain structures could be observed, namely choroid plexus (Fig. 2i) and even immature retina (Fig. 2j). Overall, all tissues examined displayed regions with dorsal cortical morphology (35 out of 35; 100%), most displayed choroid plexus (25 out of 35; 71%) and several displayed ventral forebrain identity as determined by NKX2-1 immunoreactivity (12 out of 35; 34%), whereas only a few displayed retinal tissue (determined by presence of retinal pigmented epithelium; 4 out of 35; 11%). These results indicate that cerebral organoids developed a variety of brain region identities organized into discrete, although interdependent, domains.

### Recapitulation of dorsal cortical organization

The most dramatic changes in brain evolution from rodent to human affect the dorsal cortex. Therefore, we analysed the organization of dorsal cortical regions within cerebral organoids. Staining for markers of RGs and newborn neurons (Fig. 3a) revealed typical organization into a layer reminiscent of the VZ with neurons located at the basal surface. Staining for TBR1 (Fig. 3b) revealed proper development of neural identity and radial migration to the developing preplate (precursor to the cortical plate). Furthermore, staining for neural progenitor and neural-specific BAF (mammalian SWI/SNF chromatin-remodelling complex) components revealed the characteristic switch in chromatin-remodelling complexes during neural fate specification<sup>27,28</sup> (Extended Data Fig. 3a). Finally, staining for the intermediate progenitor marker TBR2 (also known as EOMES) (Fig. 3c) revealed the presence of intermediate progenitors adjacent to the VZ. Thus, dorsal cortical tissues displayed typical progenitor zone organization.

In both mice and humans, cortical progenitors undergo a stereotypical nuclear movement called interkinetic nuclear migration (IKNM). Mitotic divisions occur at the apical surface of the VZ whereas the nuclei of cells in S phase are located on the basal side of the VZ<sup>29</sup>. We stained for the mitotic marker phospho-histone H3 (Fig. 3d) and observed most of the cells dividing at the apical surface. Similar observations were evident when we stained for phospho-vimentin (p-vimentin, Fig. 3e), a marker of mitotic RGs. In addition, as this marker labels the entire cell, we could observe basal cellular processes typical of RGs, which extended to the outer surface of these tissues (Extended Data Fig. 3b). Thus, RGs of cerebral organoids exhibited typical behaviour and morphological features.

To examine this in more detail, we used a method to label individual RGs for morphology and live imaging experiments. In the mouse brain, individual cells can be labelled by *in utero* electroporation of fluorescent-protein-expressing plasmids. Similarly, we injected green fluorescent protein (GFP) plasmid into fluid-filled cavities of cerebral organoids and electroporated RGs adjacent to these ventricle-like cavities (Extended Data Fig. 3c). This approach led to reproducible expression of GFP in RGs, revealing typical morphology at various stages of development: early pseudostratified neuroepithelium (Extended Data Fig. 3d) followed by later bipolar morphology with extended apical and basal processes (Extended Data Fig. 3e, f).

To test for IKNM, we performed live imaging of GFP-electroporated RGs in cerebral organoids and observed many examples of RGs that displayed movement of the cell body along the apical and basal processes

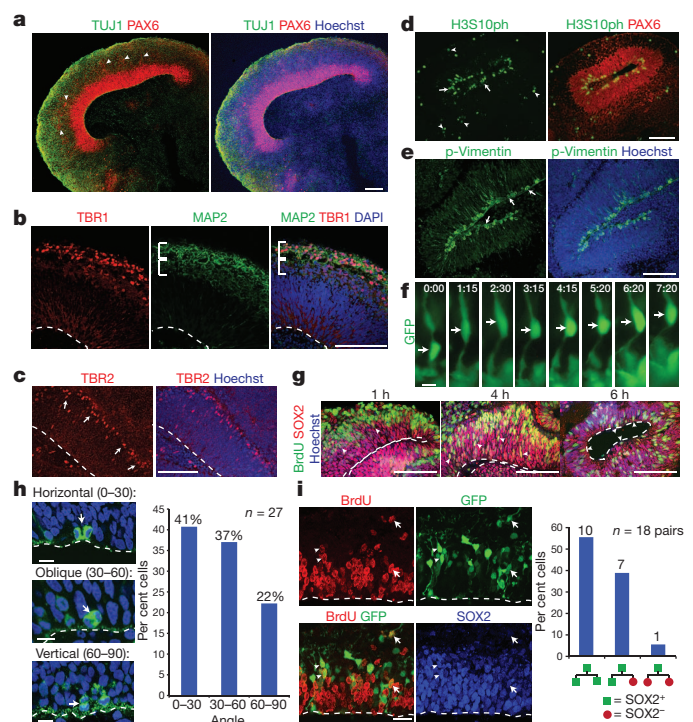


**Figure 3 | Stereotypical organization and behaviour of progenitors.**

**a**, Immunohistochemistry for neurons (TUJ1, green) and RGs (PAX6, red) in a large dorsal cortical region. Note the additional PAX6<sup>+</sup> RGs located outside the VZ (arrowheads), reminiscent of oRGs. **b**, Staining for the preplate marker TBR1 (red) and neuronal marker MAP2 (green) revealing superficial preplate (upper bracket) and underlying neuronal intermediate zone-like layer (lower bracket). **c**, Staining for the intermediate progenitor marker TBR2 (red) revealing SVZ localization of intermediate progenitors (arrows). **d**, Staining for phospho-histone H3 (H3S10ph green) to mark RG (PAX6<sup>+</sup>) in mitosis. Arrows mark apical surface divisions; arrowheads mark SVZ divisions. **e**, p-Vimentin (green) staining for mitotic RG, which primarily divide at the apical surface (arrows). **f**, Frames from live imaging of GFP-electroporated RGs showing cell body movement (arrows). Time shown in h:min. **g**, BrdU pulse-chase revealing progressive IKNM of BrdU-labelled nuclei (green, arrowheads) from basal VZ (1 h) to a more apical position (4–6 h). **h**, Quantification of RG division orientation displayed in bins of 0–30 (horizontal), 30–60 (oblique) and 60–90 (vertical) degrees.  $n = 27$  anaphase cells from five cerebral cortical tissues. **i**, Lineage tracing in GFP-electroporated and BrdU-pulsed tissues to mark daughter cell pairs following 16-h chase revealing symmetric (arrowheads) and asymmetric (arrows) fates indicated by SOX2 staining (blue). Quantification for 18 cell pairs from three cortical tissues. Numbers above bars are absolute cell numbers. Dashed line indicates apical surface (**b**, **c**, **g**, **h**, **i**). Scale bars, 100  $\mu\text{m}$  (**a–e**, **g**), 10  $\mu\text{m}$  (**f**, **h**) and 20  $\mu\text{m}$  (**i**).

(Fig. 3f and Supplementary Video 1). Furthermore, we performed pulse-chase experiments with the S-phase marker BrdU (Fig. 3g) and could observe a shift in RG nuclei from outer VZ localization towards the apical surface with time (Fig. 3g).

RGs in the VZ of rodents exhibit biased spindle orientation, predominantly horizontal, parallel to the ventricular surface<sup>30–33</sup>. To examine whether RGs in human cerebral organoids exhibited a similar orientation bias, we used p-vimentin staining to examine the plane of division in mitotic RGs (Extended Data Fig. 3g). We observed mainly horizontal orientations (41%) (Fig. 3h), somewhat similar to the orientation bias observed in other mammals. However, we also observed abundant oblique (37%) and vertical (22%) orientations, which were more abundant in these human tissues than has been described for rodent neocortex<sup>30,31,34,35</sup>. Interestingly, these measurements reflected the same trend recently described in the human brain<sup>36</sup>, suggesting that the cerebral organoids could recapitulate aspects of human cortical development.

We examined further the fate potential of these divisions to test whether organoid RGs could divide symmetrically and/or asymmetrically. We

performed electroporation of GFP followed by a short 1-h BrdU pulse and a 16-h chase to lineage trace divisions of a small minority of cells. We examined double-labelled daughter-cell pairs and could observe both symmetric proliferative fate outcomes, as well as asymmetric outcomes (Fig. 3i). This suggests that the RGs in these human tissues can undergo both symmetric and asymmetric divisions.

### Formation of functional cerebral cortical neurons

The formation of the radially organized cortical plate begins with the formation of its precursor, the preplate. To test for this initial organization, we stained 30-day organoids for TBR1, a marker of the preplate<sup>37</sup>, as well as MAP2, a neuronal marker<sup>38</sup> (Fig. 4a). This revealed the presence of a basal neural layer reminiscent of the preplate, and an apically adjacent region reminiscent of the intermediate zone. Furthermore, we could observe reelin<sup>+</sup> neurons along the basal surface, suggesting the presence of Cajal–Retzius cells, a cell population important in the generation of cortical plate architecture<sup>39</sup>.

The stereotypical layered structure of the mammalian cortical plate is generated inside-out with later-born neurons migrating through existing layers to populate more superficial layers<sup>40</sup>. Although previous methods of deriving cortical neurons have been able to generate distinct layer identities<sup>20,23,41</sup>, they have been unable to recapitulate this spatial separation. To test whether this organization could be recapitulated in cerebral organoids, we stained for cortical layer markers. In less-developed tissues (30 day), early-born CTIP2 (also known as BCL11B)<sup>+</sup> neurons were located adjacent and internal to the TBR1<sup>+</sup> preplate, suggesting initiation of cortical plate layer formation (Extended Data Fig. 4a). Furthermore, neurons exhibited rudimentary separation into an early-born deep layer (CTIP2<sup>+</sup>) and a late-born superficial layer (SATB2<sup>+</sup> and BRN2 (also known as POU3F2)<sup>+</sup>) (Extended Data Fig. 4b), which became more distinct as tissues developed (75 days) (Fig. 4c). Finally, a cell-poor region reminiscent of the marginal zone was also evident (Extended Data Fig. 1b). Notably, although this modest spatial separation was an improvement upon other *in vitro* methods, organoids could not recapitulate the same degree of mature layer organization as *in vivo*, suggesting that further cues are needed to generate the complex stereotypical layer II–VI organization.

*In vivo*, dorsal cortical neurons mature and extend long-range axons<sup>42</sup>. To test for these characteristics, we performed GFP electroporation and examined neuronal morphology. GFP-labelled axon projections displayed complex branching and growth cone behaviour (Extended Data Fig. 4c) and projected long-range axons in a manner reminiscent of axon bundling (Extended Data Fig. 4d)<sup>43</sup>.

Finally, we tested whether neurons within cerebral organoids could exhibit neural activity by performing calcium dye imaging to detect Ca<sup>2+</sup> oscillations<sup>44</sup>, which revealed spontaneous calcium surges in individual cells (Fig. 4d, Extended Data Fig. 4e and Supplementary Videos 2, 3). Furthermore, we applied exogenous glutamate (Fig. 4e) and observed more frequent calcium spikes, indicating glutamatergic receptor activity. Finally, we performed action potential blockade by application of tetrodotoxin and observed dampened calcium surges, indicating that calcium spikes were dependent upon neuronal activity (Fig. 4f).

### Recapitulation of human cortical organization

Human brain development exhibits unique progenitor zone organization<sup>2,7</sup>. To test whether features of human brain development were recapitulated in cerebral organoids, we examined the distribution of SOX2<sup>+</sup> progenitors and observed a population displaced from the apical surface (Fig. 5a and Extended Data Fig. 5a), consistent with an oRG identity. Furthermore, these fairly abundant oRGs appeared separated from the apical VZ by a TUJ1<sup>+</sup> fibre layer (Fig. 5a) reminiscent of the IFL. This organization suggests that human cerebral organoids could recapitulate at least some aspects of human cortical development.

To rule out the possibility that this OSVZ-like organization was an *in vitro* artefact, we adapted the method to mouse ES cells to generate

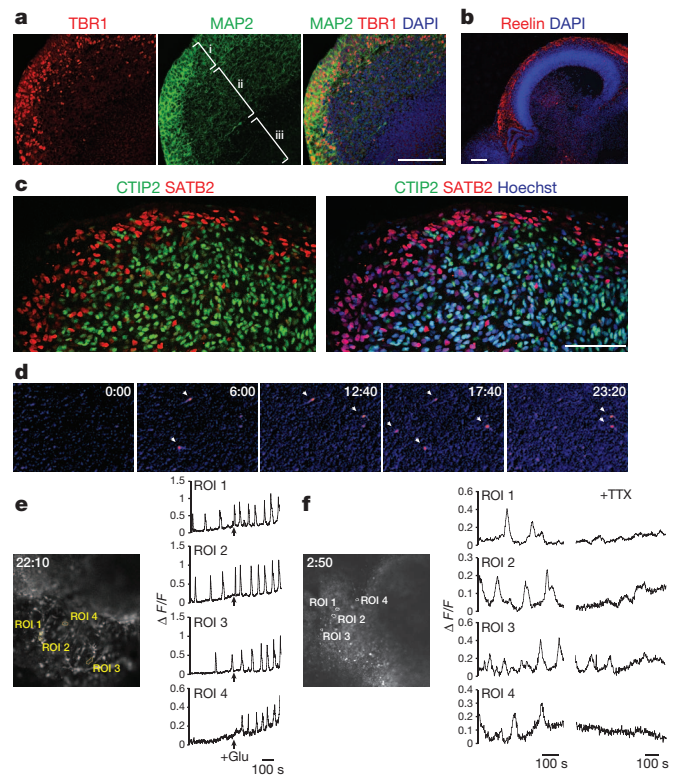


**Figure 4 | Organization and maturation of cerebral cortical neurons.** **a**, Immunohistochemical staining at day 30 showing preplate (TBR1) with early signs of radial organization (MAP2, bracket i) and the presence of an intermediate zone-like layer (bracket ii) adjacent to the VZ/SVZ (bracket iii). DAPI marks nuclei (blue). **b**, Reelin staining indicating Cajal–Retzius cells along the basal surface of dorsal cortical tissue. **c**, Staining for early-born (CTIP2) and late-born (SATB2) neurons at 75 days differentiation reveals separation and rudimentary inside-out organization. **d**, False-colour heat map frames from Fluo-4 calcium live imaging revealing spontaneous calcium surges (arrowheads). Time is displayed in min:sec. **e**, Single-cell tracings of calcium surges with glutamate application (regions of interest (ROI) outlined in left panel) as measured by change in fluorescence (arbitrary units). Arrows mark the time of addition of glutamate. **f**, Single-cell tracing (ROIs marked in image at left) of calcium surges before (left) and after (right) the addition of tetrodotoxin (TTX). Scale bars, 100  $\mu$ m.

mouse cerebral organoids and examined whether a similar organization was present (Extended Data Fig. 5b, c). We observed much smaller cortical tissues in mouse organoids compared with humans, and only occasional oRGs that did not accumulate in an OSVZ-like region. These results indicate that OSVZ- and IFL-like layers are specific to human organoids.

We performed p-vimentin staining to examine the morphology of human oRGs, which revealed basal processes but a lack of apical processes (Fig. 5b), a hallmark of oRGs<sup>3,4</sup>. This suggests that these basally displaced SOX2<sup>+</sup> and p-vimentin<sup>+</sup> progenitors indeed represent human oRGs. We also examined the division mode of oRGs and could identify daughter cell pairs in which only one daughter cell maintained SOX2 expression (Fig. 5c), suggesting asymmetric division. Furthermore, we measured spindle orientation and found that nearly all oRGs divided vertically (Fig. 5d). This division mode is remarkably similar to the findings recently described in human brain slice cultures<sup>36</sup>, suggesting recapitulation of human oRG behaviour in cerebral organoids.

### Cerebral organoids model human microcephaly

Because disorders affecting human brain development have often proved difficult to recapitulate in animal models, we tested whether organoids could be used to model neurodevelopmental disorders. We identified a patient with severe microcephaly ( $-13.2$  s.d. below mean for age and sex, Fig. 6a) and reduced stature ( $-6.7$  s.d., Supplementary Text and

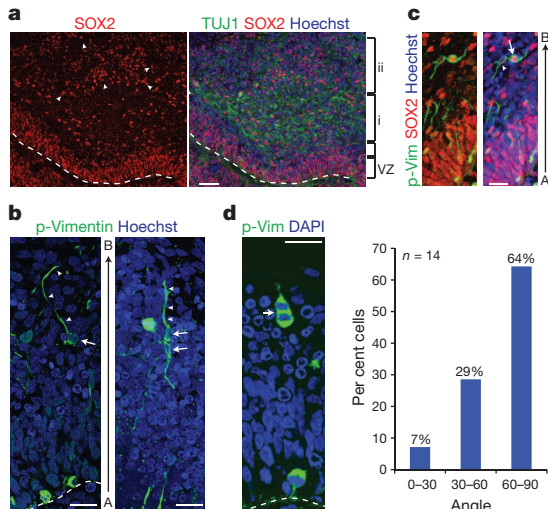


**Figure 5 | Cerebral organoids produce oRGs with typical morphology and behaviour.** **a**, Immunohistochemical staining for RGs (SOX2) and neuronal processes (TUJ1) reveals the presence of oRGs (arrowheads) organized similar to human cortical development (OSVZ-like layer, bracket ii) separated from the VZ by a layer of TUJ1<sup>+</sup> fibres similar to IFL (bracket i). **b**, Staining for p-vimentin revealing dividing oRGs (arrows) with typical morphology: possessing a basal process (arrowheads) but lacking an apical process. Right, a daughter cell pair showing unequal inheritance of the basal process. Apical–basal orientation indicated by A→B. **c**, Staining for p-vimentin in a recently divided daughter cell pair with asymmetric fates: one oRG (arrow, SOX2<sup>+</sup>), whereas the other lacks SOX2 expression (arrowhead). **d**, Orientation of division of a mitotic oRG in anaphase revealing vertical (60–90 degrees) orientation relative to the apical surface (dashed line). Quantification of spindle orientation for 14 anaphase oRGs from 6 different cortical tissues. Scale bars, 50 μm (a), 20 μm (b–d).

Extended Data Fig. 6a), who, as determined through exome sequencing and confirmed by capillary sequencing (Fig. 6b), had compound heterozygous truncating mutations in *CDK5RAP2*. Skin fibroblasts from this patient revealed a loss of the CDK5RAP2 protein (Fig. 6c and Extended Data Fig. 6b) suggesting loss of function, consistent with previously reported *CDK5RAP2* mutations in primary microcephaly patients<sup>45,46</sup>.

We performed reprogramming of patient skin fibroblasts using lentiviral delivery of the four well-described reprogramming factors: OCT4, SOX2, MYC and KLF4 (refs 47, 48). We generated many independent clones of iPS cells and characterized four of these for morphology and pluripotency. All four lines exhibited similar doubling times and colony morphology that was indistinguishable from control iPS cells (Extended Data Fig. 7a). All lines could form embryoid bodies and stained positive for the pluripotency marker alkaline phosphatase (Extended Data Fig. 7b).

We performed cerebral organoid culture from all four lines and observed smaller embryoid bodies, which when transferred to neural induction failed to develop further (Extended Data Fig. 7c). We proposed that because the patient also displayed reduced stature, perhaps overall embryoid body growth was perturbed. Therefore, in order to allow the embryoid bodies to develop to a comparable size as control, we modified the protocol slightly by increasing the initial iPS cell number. This modification allowed for the formation of neuroectoderm and subsequent neural tissue for analysis, which revealed smaller neuroepithelial tissues and a large degree of neuronal outgrowth compared with control tissues (Fig. 6d and Extended Data Fig. 7d). Immunohistochemical staining for progenitors and neurons revealed smaller neural tissues with only very few progenitor regions (Fig. 6e). These overall smaller neural tissues were reminiscent of the reduced brain size seen in the patient.

These patient-derived cerebral organoids provided a unique opportunity to examine the cause of the hypoplasia seen in microcephaly. We therefore examined an earlier stage (22 days) and observed that, whereas control tissues displayed abundant, large neuroepithelial tissues composed

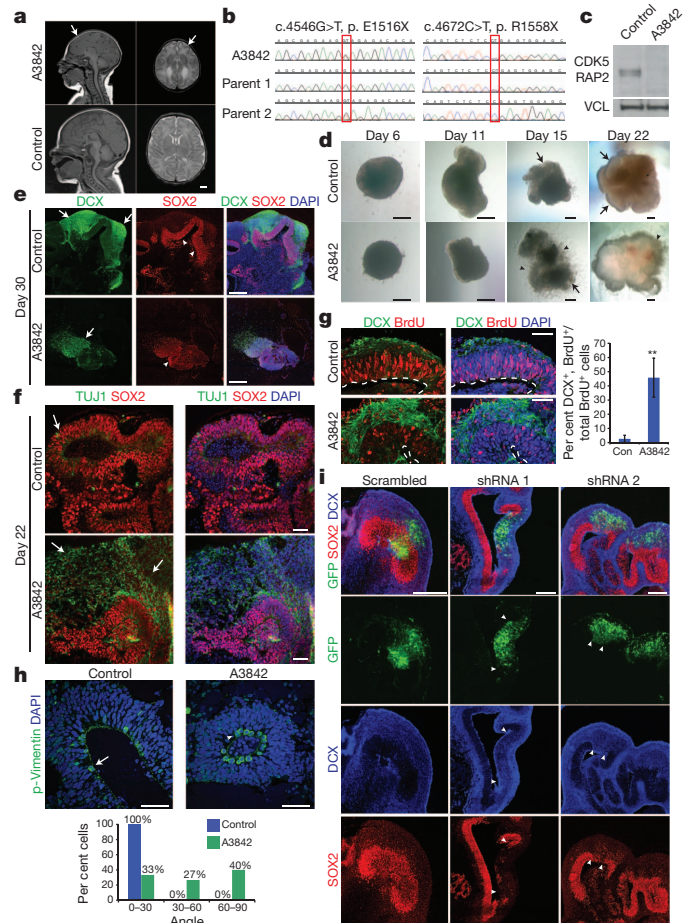


**Figure 6 | Cerebral organoid modelling of microcephaly.** **a**, Magnetic resonance imaging scan from patient A3842 taken at birth (top) compared with age-matched control (bottom) showing brain and head size reduction and simplified cortical folding (arrows). Sagittal T1 (left) and axial T2 (right) images. Scale bar, 1 cm. **b**, Sequencing chromatograms demonstrating compound heterozygous nonsense mutations inherited from each parent. **c**, CDK5RAP2 protein is undetectable on immunoblotting of patient cell lysate (A3842) compared with control skin fibroblasts. Vinculin (VCL), loading control. **d**, Representative bright-field images of control and patient-derived cerebral organoids (A3842 line 1M, all lines shown in Extended Data Fig. 7d) at 6, 11, 15 and 22 days of differentiation. Control exhibits large fluid-filled cortical regions (arrows), whereas patient-derived exhibits increased outgrowth (arrowheads). **e**, Immunohistochemistry in control and patient-derived (10M) tissues at day 30 of differentiation revealing fewer neurons (DCX, arrows) and smaller progenitor zones (SOX2, arrowheads). **f**, Staining at day 22 showing increased neurons (TUJ1, arrows) in patient-derived tissue (14B). **g**, BrdU pulse-chase in control and patient-derived organoids (14B) showing higher percentage of BrdU<sup>+</sup> cells with neural identity and less in the VZ compared with control. Results quantified on right. Error bars are s.d. **\*\*P** < 0.01, Student's *t*-test. *n* = 3 organoids for each condition (300 cells total for control, 204 cells for patient). **h**, p-Vimentin staining in control and patient-derived tissues (14B) showing RG mitotic divisions. Control RGs at anaphase divided exclusively horizontal (0–30 degree angle, arrow) whereas patient RGs displayed many oblique and vertical orientations (arrowhead). Results quantified on right (*P* < 0.01, 2 × 3 Fisher's exact test, *n* = 11 cells for control, *n* = 15 cells for patient-derived, from >5 cortical regions each). **i**, Human ES cell organoids co-electroporated with GFP and scrambled or *CDK5RAP2* shRNAs and examined after 5 days. Electroporated regions (demarcated by arrowheads) exhibit loss of SOX2<sup>+</sup> progenitors and increased DCX<sup>+</sup> neurons. Scale bars, 200 μm (d, e, i), 50 μm (f–h).

of progenitors, patient-derived tissues displayed only occasional neuroepithelial regions (Extended Data Fig. 7e). Furthermore, these tissues displayed decreased RGs and increased neurons compared with control (Fig. 6f and Extended Data Fig. 7f), suggesting premature neural

differentiation. To test this possibility, we performed BrdU pulse-chase experiments (Fig. 6g), which revealed a marked increase in the number of BrdU<sup>+</sup>/doublecortin (DCX)<sup>+</sup> cells in patient organoids, consistent with premature neurogenic non-proliferative divisions.

We next examined radial glial spindle orientation and observed that, whereas control tissues at this early stage (22 days) displayed exclusively horizontal orientations (Fig. 6h), patient organoids displayed many oblique and vertical oriented spindles (Fig. 6h). These results could explain the patient tissue phenotype because precise horizontal orientation of the spindle is necessary for early symmetric expansion of neural stem cells<sup>32</sup>.

Finally, we tested whether the phenotype could be rescued by reintroducing CDK5RAP2 protein. We performed co-electroporation of GFP and CDK5RAP2 into day-12 patient organoids and examined 6 days later. Because high overexpression of CDK5RAP2 was toxic (data not shown), the cells with high GFP signal did not survive to this time point. However, we could observe regions in CDK5RAP2-electroporated tissues with larger neuroepithelium compared with tissues electroporated only with GFP (Extended Data Fig. 7g). This effect could be due to surviving cells with a low level of CDK5RAP2 re-expression. Supporting this interpretation, staining for GFP (Extended Data Fig. 7h) revealed many low-level GFP<sup>+</sup> cells in CDK5RAP2-co-electroporated patient organoids with radial glial morphology (54% ± 2 s.e.m.; *n* = 74 cells from three tissues). By contrast, GFP<sup>+</sup> cells in patient organoids electroporated with GFP alone exhibited mainly neuronal morphology with significantly fewer RG (19% ± 11 s.e.m.; *n* = 102 cells from three tissues; *P* < 0.05, Student's *t*-test). Thus, we conclude that the phenotype is specific to the loss of CDK5RAP2.

As a further independent approach, we performed RNAi knock-down of *CDK5RAP2* by co-electroporating GFP with two independent shRNAs found to knock down endogenous *CDK5RAP2* (Extended Data Fig. 8a). Both shRNAs led to a considerable loss of SOX2<sup>+</sup> progenitors and an increase in DCX<sup>+</sup> neurons (Fig. 6i and Extended Data Fig. 8b), reflecting a statistically significant increase in neuron production rather than progenitor maintenance (Extended Data Fig. 8c). These findings support the conclusion that loss of CDK5RAP2 leads to premature neural differentiation at the expense of progenitors.

## Discussion

We have established a novel approach to studying human neurodevelopmental processes through *in vitro* culture of cerebral organoids from human pluripotent stem cells. This method recapitulates not only fundamental mechanisms of mammalian neurodevelopment, but also displays characteristics of human brain development. We are hopeful that this method will allow for the study of a variety of neurodevelopmental processes specific to human brain development.

Furthermore, a primary goal in neuroscience is to understand the roots of human neurological disease. We have modelled at least some aspects of microcephaly in these cerebral organoids. The finding that progenitor zones in patient-derived tissues display premature neural differentiation at the expense of early progenitors supports a model in which the founder population of RG progenitors fails to properly expand in patient tissues, thereby leading to an overall smaller brain. This may also explain why mouse models have been unable to recapitulate the severity of the disorder in humans. It is proposed that the mouse founder population of neural progenitors do not undergo expansion to the same extent as in humans before the onset of neurogenesis<sup>7</sup>. Thus, a disruption of the founder population in mice would not lead to as severe an effect as that seen in humans. Overall, our findings suggest that we can use this *in vitro* culture system to model aspects of human neurodevelopment and neurological disease and hopefully provide novel insight into the pathogenesis of these disorders.

## METHODS SUMMARY

For cerebral organoid differentiation, pluripotent stem cells were dissociated from mouse embryonic fibroblasts by dispase treatment followed by trypsinization to

generate single cells. In total, 4,500 cells were plated in each well of an ultra-low binding 96-well plate (Corning) in human ES media with low concentration basic fibroblast growth factor (4 ng ml<sup>-1</sup>) and 50 μM Rho-associated protein kinase (ROCK) inhibitor<sup>49</sup> (Calbiochem). Embryoid bodies were fed every other day for 6 days then transferred to low-adhesion 24-well plates (Corning) in neural induction media containing Dulbecco's modified eagle medium (DMEM)/F12, 1:100 N2 supplement (Invitrogen), Glutamax (Invitrogen), minimum essential media-essential amino acids (MEM-NEAA) and 1 μg ml<sup>-1</sup> heparin<sup>50</sup> (Sigma). The neuroepithelial tissues were fed every other day for 5 days. On day 11, tissues were transferred to droplets of Matrigel (BD Biosciences) by pipetting into cold Matrigel on a sheet of Parafilm with small 3 mm dimples. These droplets were allowed to gel at 37 °C, removed from the Parafilm and grown in differentiation media containing a 1:1 mixture of DMEM/F12 and Neurobasal containing 1:200 N2 supplement (Invitrogen), 1:100 B27 supplement without vitamin A (Invitrogen), 3.5 μl l<sup>-1</sup> 2-mercaptoethanol, 1:4,000 insulin (Sigma), 1:100 Glutamax (Invitrogen), 1:200 MEM-NEAA. After 4 days of stationary growth, the droplets were transferred to a spinning bioreactor containing differentiation media as above, except B27 supplement with vitamin A (Invitrogen) was used.

**Online Content** Any additional Methods, Extended Data display items and Source Data are available in the online version of the paper; references unique to these sections appear only in the online paper.

Received 19 December 2012; accepted 2 August 2013.

Published online 28 August 2013.

- Götz, M. & Huttner, W. B. The cell biology of neurogenesis. *Nature Rev. Mol. Cell Biol.* **6**, 777–788 (2005).
- Zecevic, N., Chen, Y. & Filipovic, R. Contributions of cortical subventricular zone to the development of the human cerebral cortex. *J. Comp. Neurol.* **491**, 109–122 (2005).
- Fietz, S. A. *et al.* OSVZ progenitors of human and ferret neocortex are epithelial-like and expand by integrin signaling. *Nature Neurosci.* **13**, 690–699 (2010).
- Hansen, D. V., Lui, J. H., Parker, P. R. L. & Kriegstein, A. R. Neurogenic radial glia in the outer subventricular zone of human neocortex. *Nature* **464**, 554–561 (2010).
- Smart, I. H. M., Dehay, C., Giroud, P., Berland, M. & Kennedy, H. Unique morphological features of the proliferative zones and postmitotic compartments of the neural epithelium giving rise to striate and extrastriate cortex in the monkey. *Cereb. Cortex* **12**, 37–53 (2002).
- Shitamukai, A., Konno, D. & Matsuzaki, F. Oblique radial glial divisions in the developing mouse neocortex induce self-renewing progenitors outside the germinal zone that resemble primate outer subventricular zone progenitors. *J. Neurosci.* **31**, 3683–3695 (2011).
- Lui, J. H., Hansen, D. V. & Kriegstein, A. R. Development and evolution of the human neocortex. *Cell* **146**, 18–36 (2011).
- Fietz, S. A. & Huttner, W. B. Cortical progenitor expansion, self-renewal and neurogenesis — a polarized perspective. *Curr. Opin. Neurobiol.* **21**, 23–35 (2011).
- Cox, J., Jackson, A. P., Bond, J. & Woods, C. G. What primary microcephaly can tell us about brain growth. *Trends Mol. Med.* **12**, 358–366 (2006).
- Megraw, T. L., Sharkey, J. T. & Nowakowski, R. S. Cdk5rap2 exposes the centrosomal root of microcephaly syndromes. *Trends Cell Biol.* **21**, 470–480 (2011).
- Barrera, J. A. *et al.* CDK5RAP2 regulates centriole engagement and cohesion in mice. *Dev. Cell* **18**, 913–926 (2010).
- Lizarraga, S. B. *et al.* Cdk5rap2 regulates centrosome function and chromosome segregation in neuronal progenitors. *Development* **137**, 1907–1917 (2010).
- Pulvers, J. N. *et al.* Mutations in mouse *Aspm* (abnormal spindle-like microcephaly associated) cause not only microcephaly but also major defects in the germline. *Proc. Natl Acad. Sci. USA* **107**, 16595–16600 (2010).
- Gruber, R. *et al.* MCPH1 regulates the neuroprogenitor division mode by coupling the centrosomal cycle with mitotic entry through the Chk1-Cdc25 pathway. *Nature Cell Biol.* **13**, 1325–1334 (2011).
- Sato, T. *et al.* Single Lgr5 stem cells build crypt-villus structures *in vitro* without a mesenchymal niche. *Nature* **459**, 262–265 (2009).
- Suga, H. *et al.* Self-formation of functional adeno-hypophysis in three-dimensional culture. *Nature* **480**, 57–62 (2011).
- Nakano, T. *et al.* Self-formation of optic cups and storable stratified neural retina from human ESCs. *Cell Stem Cell* **10**, 771–785 (2012).
- Eiraku, M. *et al.* Self-organizing optic-cup morphogenesis in three-dimensional culture. *Nature* **472**, 51–56 (2011).
- Eiraku, M. & Sasai, Y. Self-formation of layered neural structures in three-dimensional culture of ES cells. *Curr. Opin. Neurobiol.* **22**, 768–777 (2012).
- Eiraku, M. *et al.* Self-organized formation of polarized cortical tissues from ESCs and its active manipulation by extrinsic signals. *Cell Stem Cell* **3**, 519–532 (2008).
- Danjo, T. *et al.* Subregional specification of embryonic stem cell-derived ventral telencephalic tissues by timed and combinatorial treatment with extrinsic signals. *J. Neurosci.* **31**, 1919–1933 (2011).
- Muguruma, K. *et al.* Ontogeny-recapitulating generation and tissue integration of ES cell-derived Purkinje cells. *Nature Neurosci.* **13**, 1171–1180 (2010).
- Mariani, J. *et al.* Modeling human cortical development *in vitro* using induced pluripotent stem cells. *Proc. Natl Acad. Sci. USA* **109**, 12770–12775 (2012).
- Xia, X. & Zhang, S.-C. Differentiation of neuroepithelia from human embryonic stem cells. *Methods Mol. Biol.* **549**, 51–58 (2009).

25. Swanson, L. W. Mapping the human brain: past, present, and future. *Trends Neurosci.* **18**, 471–474 (1995).
26. Bedogni, F. *et al.* Tbr1 regulates regional and laminar identity of postmitotic neurons in developing neocortex. *Proc. Natl Acad. Sci. USA* **107**, 13129–13134 (2010).
27. Yoo, A. S. *et al.* MicroRNA-mediated conversion of human fibroblasts to neurons. *Nature* **476**, 228–231 (2011).
28. Lessard, J. *et al.* An essential switch in subunit composition of a chromatin remodeling complex during neural development. *Neuron* **55**, 201–215 (2007).
29. Willardsen, M. I. & Link, B. A. Cell biological regulation of division fate in vertebrate neuroepithelial cells. *Dev. Dyn.* **240**, 1865–1879 (2011).
30. Chenn, A. & McConnell, S. K. Cleavage orientation and the asymmetric inheritance of Notch1 immunoreactivity in mammalian neurogenesis. *Cell* **82**, 631–641 (1995).
31. Konno, D. *et al.* Neuroepithelial progenitors undergo LGN-dependent planar divisions to maintain self-renewability during mammalian neurogenesis. *Nature Cell Biol.* **10**, 93–101 (2008).
32. Yingling, J. *et al.* Neuroepithelial stem cell proliferation requires LIS1 for precise spindle orientation and symmetric division. *Cell* **132**, 474–486 (2008).
33. Postiglione, M. P. *et al.* Mouse inscuteable induces apical-basal spindle orientation to facilitate intermediate progenitor generation in the developing neocortex. *Neuron* **72**, 269–284 (2011).
34. Smart, I. H. Proliferative characteristics of the ependymal layer during the early development of the mouse neocortex: a pilot study based on recording the number, location and plane of cleavage of mitotic figures. *J. Anat.* **116**, 67–91 (1973).
35. Zamenhof, S. Quantitative studies of mitoses in fetal rat brain: orientations of the spindles. *Brain Res.* **428**, 143–146 (1987).
36. LaMonica, B. E., Lui, J. H., Hansen, D. V. & Kriegstein, A. R. Mitotic spindle orientation predicts outer radial glial cell generation in human neocortex. *Nature Commun.* **4**, 1665 (2013).
37. Hevner, R. F. *et al.* Tbr1 regulates differentiation of the preplate and layer 6. *Neuron* **29**, 353–366 (2001).
38. Shafit-Zagardo, B. & Kalcheva, N. Making sense of the multiple MAP-2 transcripts and their role in the neuron. *Mol. Neurobiol.* **16**, 149–162 (1998).
39. Frotscher, M. Cajal-Retzius cells, Reelin, and the formation of layers. *Curr. Opin. Neurobiol.* **8**, 570–575 (1998).
40. Tsai, L.-H. & Gleeson, J. G. Nucleokinesis in neuronal migration. *Neuron* **46**, 383–388 (2005).
41. Gaspard, N. *et al.* An intrinsic mechanism of corticogenesis from embryonic stem cells. *Nature* **455**, 351–357 (2008).
42. De Carlos, J. A. & O'Leary, D. D. Growth and targeting of subplate axons and establishment of major cortical pathways. *J. Neurosci.* **12**, 1194–1211 (1992).
43. Chédotal, A. Further tales of the midline. *Curr. Opin. Neurobiol.* **21**, 68–75 (2011).
44. Sato, T. R., Gray, N. W., Mainen, Z. F. & Svoboda, K. The functional microarchitecture of the mouse barrel cortex. *PLoS Biol.* **5**, e189 (2007).
45. Bond, J. *et al.* A centrosomal mechanism involving CDK5RAP2 and CENPJ controls brain size. *Nature Genet.* **37**, 353–355 (2005).
46. Pagnamenta, A. T. *et al.* A novel nonsense *CDK5RAP2* mutation in a Somali child with primary microcephaly and sensorineural hearing loss. *Am. J. Med. Genet.* **158A**, 2577–2582 (2012).
47. Takahashi, K. & Yamanaka, S. Induction of pluripotent stem cells from mouse embryonic and adult fibroblast cultures by defined factors. *Cell* **126**, 663–676 (2006).
48. Okita, K., Ichisaka, T. & Yamanaka, S. Generation of germline-competent induced pluripotent stem cells. *Nature* **448**, 313–317 (2007).
49. Watanabe, K. *et al.* A ROCK inhibitor permits survival of dissociated human embryonic stem cells. *Nature Biotechnol.* **25**, 681–686 (2007).
50. Hu, B.-Y. & Zhang, S.-C. Directed differentiation of neural-stem cells and subtype-specific neurons from hESCs. *Methods Mol. Biol.* **636**, 123–137 (2010).

**Supplementary Information** is available in the online version of the paper.

**Acknowledgements** We are grateful to members of the Knoblich laboratory for technical expertise and feedback, A. Peer, P. Moeseneder and N. Corsini for experimental support and M. Repic for help with establishing organoid electroporations. We also thank the Stem Cell and BioOptics core facilities of IMBA/IMP for technical support. We would especially like to thank the patients and their families for participating in this study. We would also like to thank S. McGurk for providing control MRI images. M.A.L. received funding from an EMBO post-doctoral fellowship and a Helen Hay Whitney post-doctoral fellowship. Work in A.P.J.'s laboratory is supported by the Medical Research Council, a starter grant from the European Research Council (ERC) and the Lister Institute for Preventative Medicine. This research was also supported in part by Wellcome Trust grant WT098051. Work in J.A.K.'s laboratory is supported by the Austrian Academy of Sciences, the Austrian Science Fund (FWF) (projects Z153-B09 and I552-B19) and an advanced grant from ERC.

**Author Contributions** M.A.L. and J.A.K. conceived the project and experimental design and wrote the manuscript. M.A.L. performed experiments and analysed data. M.R., C.-A.M. and D.W. performed experiments and analysed data under the supervision of J.A.K., J.M.P. and A.P.J. L.S.B., M.E.H. and T.H. performed patient diagnosis and provided MRIs coordinated by A.P.J. J.A.K. directed and supervised the project.

**Author Information** Reprints and permissions information is available at [www.nature.com/reprints](http://www.nature.com/reprints). The authors declare no competing financial interests. Readers are welcome to comment on the online version of the paper. Correspondence and requests for materials should be addressed to J.A.K. ([juergen.knoblich@imba.oew.ac.at](mailto:juergen.knoblich@imba.oew.ac.at)).

## METHODS

**Plasmid constructs and materials.** GFP plasmid used for co-electroporation with shRNA and for live imaging was pCAG-GFP (Addgene plasmid 11150)<sup>51</sup>. shRNAs targeting human *CDK5RAP2* were cloned using pSuper shRNA expression strategy (OligoEngine). Targeting sequences were as follows: shRNA 1, 5'-AGGA CGTGTGCTTCAGAAAT-3'; shRNA 2, 5'-AGAGTCAGCCTTCTGCTAAAG-3'; shRNA 3, 5'-GTGGAAGATCTCCTAACTAAA-3'; shRNA 4, 5'-ACTATGAGA CTGCTCTATCAG-3'. The *CDK5RAP2* expression construct was generated using the Gateway system (Invitrogen) by PCR amplification of *CDK5RAP2* from MGC human *CDK5RAP2* cDNA (clone ID: 9052276) using the primers with AttB sites: forward, 5'-GGGGACAAGTTGTACAAAAAGCAGGCTTCATGATGGACT TGGTGTGGAGA-3'; reverse, 5'-GGGGACCACTTTGTACAAGAAAGCTG GGTCACTTTATTGGCTGAAAGTTCTTCTC-3'. *CDK5RAP2* was cloned into destination vector pcDNA3.1/nV5-DEST.

**Cerebral organoid culture conditions.** Human H9 ES (WA09) cells were obtained from WiCell at passage 26 with verified normal karyotype and contamination-free. iPS cells were obtained from System Biosciences (SC101A-1) verified pluripotent and contamination-free. All human pluripotent stem cell lines were regularly checked and confirmed negative for mycoplasma. Pluripotent stem cells were maintained on CF-1-gamma-irradiated mouse embryonic stem cells (MEFs) (Global Stem) according to WiCell protocols. On day 0 of organoid culture, ES cells or iPS cells at less than passage 50 were dissociated from MEFs by dispase treatment and MEFs were removed by gravity separation of stem cell colonies from MEFs before trypsinization of stem cells to generate single cells. In total, 4,500 cells were then plated in each well of an ultra-low-binding 96-well plate (Corning) in human ES media with low concentration basic fibroblast growth factor (4 ng ml<sup>-1</sup>) and 50 μM Rho-associated protein kinase (ROCK) inhibitor<sup>49</sup> (Calbiochem).

Embryoid bodies were fed every other day for 6 days then transferred to low-adhesion 24-well plates (Corning) in neural induction media containing Dulbecco's modified eagle medium (DMEM)/F12, 1:100 N2 supplement (Invitrogen), Glutamax (Invitrogen), minimum essential media-nonsessential amino acids (MEM-NEAA) and 1 μg ml<sup>-1</sup> heparin<sup>50</sup> (Sigma). These began forming neuroepithelial tissues, which were fed every other day for 5 days. On day 11 of the protocol, tissues were transferred to droplets of Matrigel (BD Biosciences) by pipetting into cold Matrigel on a sheet of Parafilm with small 3 mm dimples. These droplets were allowed to gel at 37 °C and were subsequently removed from the Parafilm and grown in differentiation media containing a 1:1 mixture of DMEM/F12 and Neurobasal containing 1:200 N2 supplement (Invitrogen), 1:100 B27 supplement without vitamin A (Invitrogen), 3.5 μl l<sup>-1</sup> 2-mercaptoethanol, 1:4,000 insulin (Sigma), 1:100 Glutamax (Invitrogen) and 1:200 MEM-NEAA.

After 4 days of stationary growth, the tissue droplets were transferred to a spinning bioreactor containing differentiation media as above except B27 supplement with vitamin A (Invitrogen) was used. Because retinoic acid has been shown to be important for neuronal differentiation *in vivo*<sup>52</sup>, we included it in the final media used to differentiate the cerebral organoids.

**Mouse organoid culture conditions.** Mouse A9 ES cells were cultured on mitomycin-C-growth-inactivated MEFs and passaged according to standard protocols<sup>53</sup>. For the generation of mouse organoids, the organoid protocol was applied with the following modifications: cells were trypsinized and 2,000 stem cells were plated in each well of an ultra-low-binding 96-well plate in differentiation medium as described in ref. 20 (medium containing 10 μM SB431542 but without DKK1). Subsequent steps were followed according to the human organoid method using identical media compositions, with the exception that for mouse tissues faster timing was used according to morphology. Embryoid bodies were transferred to neural induction medium on day 4, embedded in Matrigel droplets on day 6, and on day 9 transferred to the spinning bioreactor.

**Organoid electroporation.** Electroporation was performed using a Petri dish tissue electrode and electro-square-porator (ECM 830), both from BTX Harvard Apparatus. A total of 3 μl of 2 μg μl<sup>-1</sup> total plasmid (GFP for live imaging, 1.8 μg μl<sup>-1</sup> shRNA plus 0.2 μg μl<sup>-1</sup> GFP for shRNA experiments) was injected in 4–5 locations within the organoid and electroporation was performed in differentiation media without antibiotics at 5 pulses, 80 V, 50-μs duration, 1-s interval. For rescue experiments, GFP expression plasmid and the *CDK5RAP2* construct were co-electroporated at equal concentrations (1 μg μl<sup>-1</sup> each).

**Live imaging in organoids.** Live imaging was performed using a LSM780 confocal laser scanning system (Zeiss) equipped with temperature and CO<sub>2</sub> control. For calcium imaging, Fluo-4 direct (Life Technologies) was prepared according to manufacturer and applied 60 min before the start of imaging. Imaging was performed at 494 nm excitation and 516 nm emission, with frames taken every 20 s for 100 frames. Data analysis of calcium imaging was performed using ImageJ (Fiji). ROIs were manually selected and mean fluorescence was calculated for each time frame. Change in fluorescence was calculated as follows:  $\Delta F/F = (F - F_{\text{basal}}) / F_{\text{background}}$ , in which  $F_{\text{basal}}$  was the lowest mean fluorescence value across imaging

and  $F_{\text{background}}$  was the average mean fluorescence across all frames. Glutamate was added by bath application to media during imaging at a final concentration 100 μM. TTX was added by bath application to media during imaging at a final concentration of 1 μM and imaging was resumed after a 10-min incubation time.

**Histology and immunofluorescence.** Tissues were fixed in 4% paraformaldehyde for 20 min at 4 °C followed by washing in PBS three times for 10 min. Tissues were allowed to sink in 30% sucrose overnight and then embedded in 10%/7.5% gelatin/sucrose and cryosectioned at 20 μm. Tissue sections were stained with haematoxylin and eosin or used for immunostaining. For immunohistochemistry, sections were blocked and permeabilized in 0.25% Triton X-100 and 4% normal donkey serum in PBS. Sections were then incubated with primary antibodies in 0.1% Triton X-100, 4% normal donkey serum at the following dilutions: N-cadherin (mouse, BD Biosciences 610920, 1:500), SOX2 (rabbit, Chemicon, AB5603, 1:300), TUJ1 (mouse, Covance MMS-435P, 1:750), TUNEL (*In situ* Cell Death Detection Kit-Fluorescein, Roche), FOXG1 (rabbit, Abcam ab18259, 1:200), EMX1 (rabbit, Sigma HPA006421, 1:50), KROX20 (rabbit, Covance PRB-236P, 1:100), PAX2 (mouse, Abnova H00005076-M01, 1:200), LMO4 (goat, Santa Cruz sc-11122, 1:50), TSHZ2 (rabbit, Sigma SAB4500379, 1:50), OTX1+2 (rabbit, Abcam ab21990, 1:200), GBX2 (goat, Santa Cruz sc22230, 1:100), AUTS2 (rabbit, Sigma HPA000390, 1:250), NKX2-1 (rabbit, Epitomics 6594-1, 1:250), PAX6 (mouse monoclonal, DSHB, 1:200), PAX6 (rabbit, Covance PRB-278P, 1:300), calretinin (mouse, Swant B63, 1:100), NRP2 (goat, RandD systems AF2215, 1:40), FZD9 (rabbit, Acris SP4153P, 1:200), PROX1 (mouse, Chemicon MAB5654, 1:200), TTR (sheep, AbD Serotec AHP1837, 1:100), TBR2 (rabbit, Chemicon AB9618, 1:500), TBR1 (rabbit, Abcam ab31940, 1:300), MAP2 (mouse, Chemicon MAB3418, 1:300), H3S10ph (rabbit, Cell Signaling Technology 9706S, 1:300), p-vimentin (mouse, MBL International D076-3S, 1:250), BrdU (rat, AbD Serotec OBT0030CX, 1:500), BAF53A (rabbit, Bethyl IHC-00287, 1:250), BAF53B (rabbit, Abcam ab140642, 1:250), reelin (mouse, Millipore MAB5366, 1:200), CTIP2 (rat, Abcam ab18465, 1:100), SATB2 (rabbit, Abcam ab34735, 1:100), DCX (goat, Santa Cruz sc-8066, 1:300), BRN2 (goat, Santa Cruz sc-6029, 1:40). Secondary antibodies used were donkey Alexa Fluor 488, 568 and 647 conjugates (Invitrogen, 1:500). For sections stained for BrdU, sections were first incubated with 2N HCl at 37 °C for 20 min followed by washing three times in PBS before blocking.

**RT-PCR.** Total messenger RNA samples were isolated from whole organoids or human ES cells in triplicate using Trizol reagent (Invitrogen). Potential contaminating DNA was removed using DNA-Free (Ambion) and 1 μg RNA was used for cDNA synthesis using SuperScript III (Life Technologies). PCR conditions and number of cycles (25–35 cycles) for each primer pair were empirically determined using human ES cDNA or human fetal brain cDNA (Invitrogen). Cycles were run at 94 °C denaturation for 30 s, 58–62 °C annealing for 45 s, depending on primer pair, and 72 °C extension for 30 s. Primer pairs used were as follows: OCT4A forward: 5'-GGAGAAGCTGGAGCAAAACC-3', reverse: 5'-TGGCTGAATACCTTCCC AAA-3'; NANOG forward: 5'-GATTTGTGGGCCTGAAGAAA-3', reverse: 5'-CTTTGGGACTGGTGAAGAA-3'; SOX1 forward: 5'-TATCTTCTGCTCCGG CTGTT-3', reverse: 5'-GGGTCTTCCCTTCCCTC-3'; PAX6 forward: 5'-AG TTCTTCGCAACCTGGCTA-3', reverse: 5'-ATTCTCTCCCCCTCCTTCTC-3'; ACTB forward: 5'-AAATCTGGCACCACCTTC-3', reverse: 5'-AGAGGCGT ACAGGGATGACA-3'; FOXG1 forward: 5'-AGGAGGGCGAGAAGAAGAAC-3', reverse: 5'-TGAAGCTAGATGCCGTTG-3'; SIX3 forward: 5'-CTATCAACA ACCCCCAACCA-3', reverse: 5'-AGCCGTGCTGTCTCTAGAAA-3'; KROX20 forward: 5'-TTGACCAGATGAACGGAGTG-3', reverse: 5'-CTTGCCCATGTA AGTGAAGGT-3'; ISL1 forward: 5'-GCTTTGTTAGGGATGGGAAA-3', reverse: 5'-ACTCGATGTGATACACCTTGA-3'.

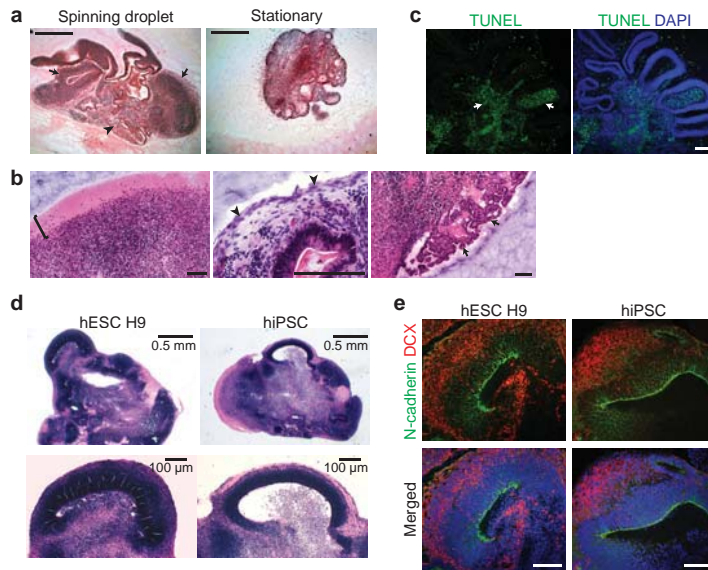
**Cell culture and western blot.** HEK293T cells were grown in 10% FBS/DMEM and split at 40% into a 6-well dish (BD Falcon) followed by transfection the next day using TurboFect (Thermo Scientific) with 5 μg plasmid DNA. Cells were lysed 2 days later and western blot was performed using rabbit anti-CDK5RAP2 (A300-554A, Bethyl Laboratories, 1:10,000) followed by blotting for mouse anti-α-tubulin (mouse, Sigma T6199, 1:10,000). Dermal fibroblasts were obtained by skin punch biopsy and were cultured in amnioMAX C-100 complete medium (Invitrogen) and maintained in a 37 °C incubator with 5% CO<sub>2</sub> and 3% O<sub>2</sub>. Cells were lysed in 50 mM Tris-HCl, pH 8, 280 mM NaCl, 0.5% NP40, 0.2 mM EDTA, 0.2 mM EGTA and 10% glycerol supplemented with protease inhibitor tablet (Roche). Protein samples were run on a 3–8% Tris-acetate gel (Invitrogen) followed by immunoblotting using rabbit anti-CDK5RAP2 (A300-554A, Bethyl Laboratories, 1:2,000) and mouse anti-vinculin (V9264, Sigma, 1:2,000). To perform immunofluorescence, patient fibroblasts were fixed in -20 °C methanol for 7 min and then blocked in PBS/1% bovine serum albumin. Cells were then incubated in rabbit anti-CDK5RAP2 (A300-554A, Bethyl Laboratories, 1:2,000) and mouse anti-CPAP (SC-81432, Santa Cruz Biotechnology, 1:100) in blocking solution. Secondary antibodies used were donkey Alexa Fluor 488 and 568 conjugates (Invitrogen, 1:500).

**Research subject and gene identification.** Genomic DNA was extracted from peripheral blood of patient 3842 and the patient's parents by standard methods. Informed consent was obtained from the family and the study approved by the Multi-centre Research Ethics Committee for Scotland (04:MRE00/19). Whole-exome capture and sequencing was performed at the Wellcome Trust Sanger Institute, UK. DNA was sheared to 150-base-pair lengths by sonification (Covaris) before whole-exome capture and amplification using the SureSelect Human All Exon 50Mb kit (Agilent). Fragments were sequenced using the Illumina HiSeq platform. 76-base-pair paired-end sequence reads were aligned to the UCSC genome browser hg19 reference sequence using BWA. Sequence variants were obtained using GenomeAnalysisTK (<http://www.broadinstitute.org/gatk/>) and annotated with transcript and protein consequence, polyphen, condel and SIFT scores. Mutations were confirmed by bi-directional sequencing of PCR products using dye terminator chemistry on an ABI 3730 capillary sequencer (Applied Biosystems).

**Patient iPS cell reprogramming.** Patient skin fibroblasts were reprogrammed using lentiviral delivery of *OCT4*, *SOX2*, *KLF4* and *MYC*. Lentivirus production: a DNA mix consisting of virus packaging vectors (tat, rev, gag/pol, 1.5 µg each, and vsv-g, 3 µg) and the loxP-flanked OKSM reprogramming vector (*OCT4*, *KLF4*, *SOX2*, *MYC*, 30 µg) were transfected into 293 cells. In brief, 112.5 µl Fugene6 was added dropwise to 2 ml DMEM under constant vortexing followed by a 10-min incubation at room temperature (22 °C). The DNA mix was added to the DMEM/Fugene6 mix while vortexing to generate the final transfection mix. After a 15-min incubation at room temperature, the transfection mix was added onto 80% confluent 293 cells, cultured in 13 ml 293 culture medium. Virus-containing medium

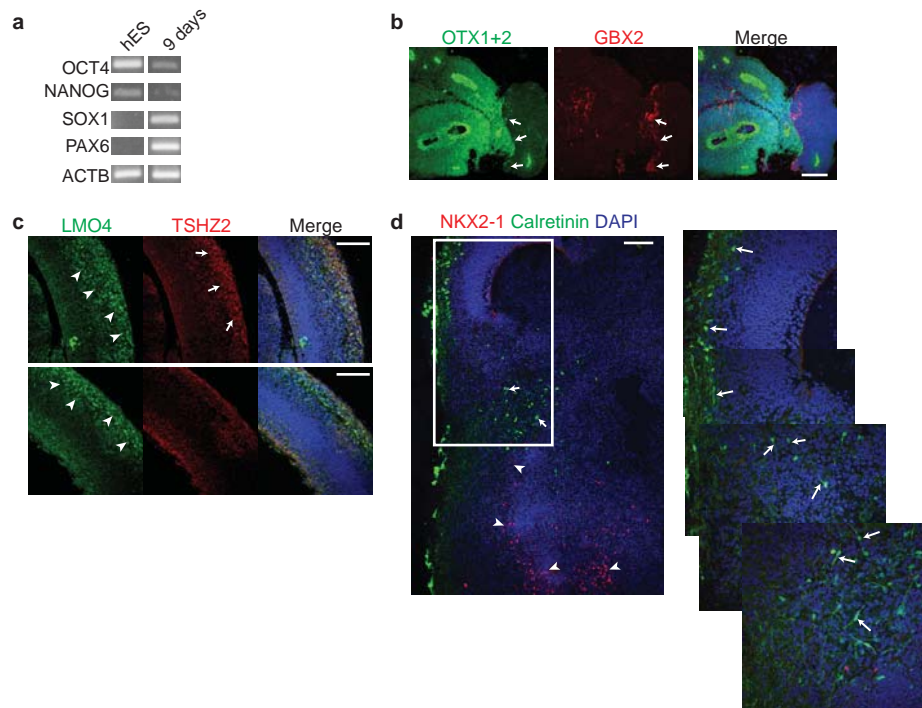
was collected and replaced with fresh medium 48, 60 and 72 h after transfection. The viral supernatant was stored at 4 °C. Reprogramming of human dermal fibroblasts:  $1 \times 10^5$  dermal fibroblasts were seeded the day before infection onto 10-cm and 6-cm 0.1% gelatin-coated culture dishes. Cells were incubated for 12 h with viral supernatant 1:1 mixed with dermal fibroblast medium supplemented with  $4 \mu\text{g ml}^{-1}$  polybrene. Thereafter, cells were washed with  $1 \times$  PBS and cultured for 2 more days in dermal fibroblast medium. After 2 days medium was switched to human iPS cell medium supplemented with  $10 \text{ ng ml}^{-1}$  basic fibroblast growth factor (peprotech, cat. no. 100-18B),  $10 \mu\text{M}$  CHIR99021 (stemgent, cat. no. 04-0004) and  $1 \mu\text{M}$  PD 0325901 (stemgent, cat. no. 04-0006) and cells cultured for 21 days. Medium was changed every day. Outgrowing colonies, identified by morphological appearance, were picked and passaged on inactivated CF-1 MEFs (global stem, cat. no. GSC-6201M). Patient-derived iPS lines were compared to control iPS cells obtained from a healthy donor (System Biosciences, SC101A-1). Alkaline phosphatase staining was performed using Vector Blue Alkaline Phosphatase Substrate Kit (Vector Laboratories, SK5300). Quantifications in patient and control iPS-cell-derived organoids were performed blinded using coded file names in ImageJ.

51. Matsuda, T. & Cepko, C. L. Electroporation and RNA interference in the rodent retina *in vivo* and *in vitro*. *Proc. Natl Acad. Sci. USA* **101**, 16–22 (2004).
52. Siegenthaler, J. A. *et al.* Retinoic acid from the meninges regulates cortical neuron generation. *Cell* **139**, 597–609 (2009).
53. Tremml, G., Singer, M. & Malavarca, R. Culture of mouse embryonic stem cells. *Curr. Protoc. Stem Cell Biol.* **1**, Unit-1C.4 (2008).



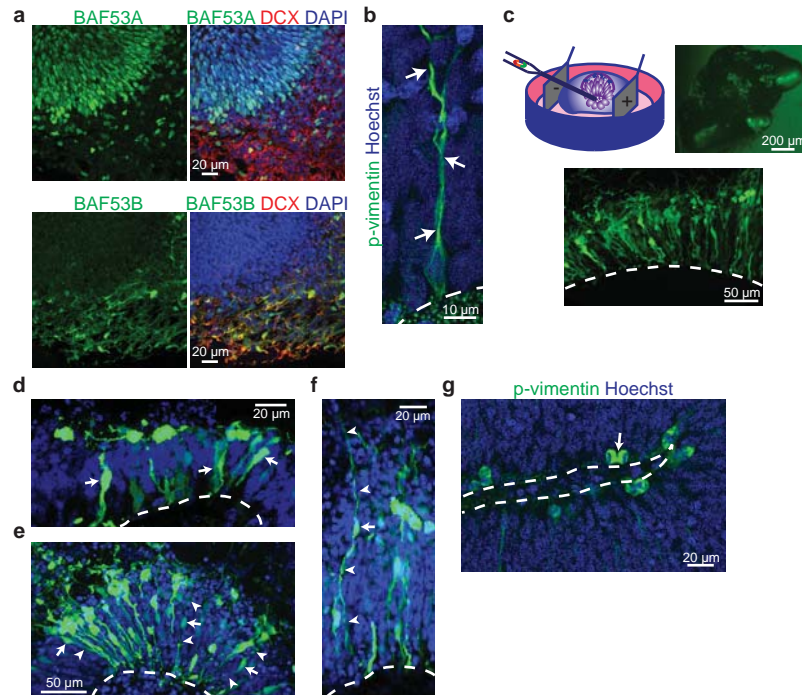
**Extended Data Figure 1 | Generation of cerebral organoids from multiple human pluripotent stem cells.** **a**, Haematoxylin and eosin staining of cerebral organoids compared with stationary culture reveals overall larger tissues with substructure reminiscent of brain regions such as forebrain cortex (arrows) and choroid plexus (arrowhead). **b**, Higher magnification images of haematoxylin and eosin stained organoids revealing layering reminiscent of the cerebral cortical molecular layer (bar), as well as tissue reminiscent of meninges (arrowheads) and choroid plexus (arrows). **c**, TUNEL staining (green) revealing cell death in the interior regions (arrows) of the cerebral organoid

with cortical regions developing along the exterior. DAPI marks nuclei (blue). **d**, Haematoxylin and eosin staining of organoids generated from human H9 ES cells as well as human iPS cells display similar size and complex morphology as well as the presence of advanced forebrain tissues, shown at higher magnification in the bottom panels. **e**, Staining for N-cadherin (green) and newborn neurons (DCX, red) in tissues generated from both human H9 ES cells and human iPS cells reveals similar organization and intact apical basal polarity in both types of tissues. Scale bars, 0.5 mm (**a**), 100  $\mu$ m (**b**, **c**, **d** bottom panels, **e**), and 0.5 mm (**d** top panels).



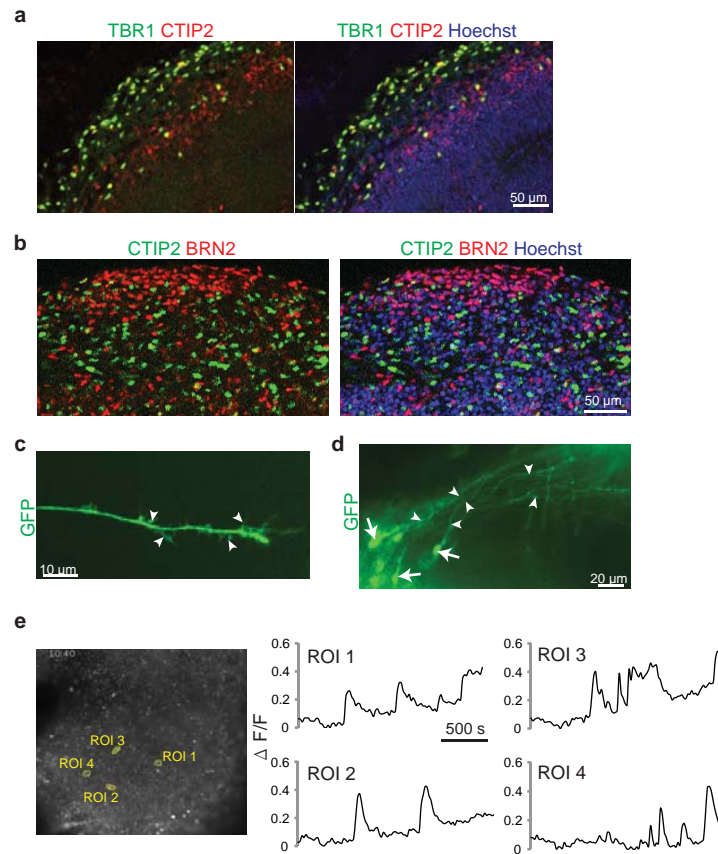
**Extended Data Figure 2 | Neural identity during differentiation of cerebral organoids.** **a**, RT-PCR for the pluripotency markers OCT4 and NANOG as well as neural identity markers SOX1 and PAX6 in undifferentiated human ES cells and following differentiation at 9 days, revealing induction of neural identity with decreased pluripotent identity at 9 days of differentiation. **b**, Immunohistochemistry for the forebrain/midbrain marker OTX1/2 (green) and the hindbrain marker GBX2 (red) at 16 days of differentiation, revealing primarily fore/midbrain identity with adjacent regions of hindbrain reminiscent of the mid-hindbrain boundary (arrows). DAPI marks nuclei (blue). **c**, Staining for the cortical lobe markers LMO4 (frontal and occipital marker, green) and TSHZ2 (occipital marker, red). Note the expected nuclear

staining (arrows and arrowheads) for both in one region (top panels) suggesting occipital identity, whereas only LMO4 staining (arrowheads) is clearly evident in another region (bottom panels), suggesting frontal identity. DAPI marks nuclei (blue). **d**, Staining for the ventral marker NKX2-1 (red) and the cortical interneuron marker calretinin (green) on an organoid containing both ventral (arrowheads) and dorsal (top left) regions within one section. Images on the right are higher magnification stitched images of the region outlined in the lower magnification image at left. Calretinin interneurons can be seen between the two regions with typical morphology of migration and redirection towards the dorsal cortex (arrows). Scale bars, 100  $\mu$ m.



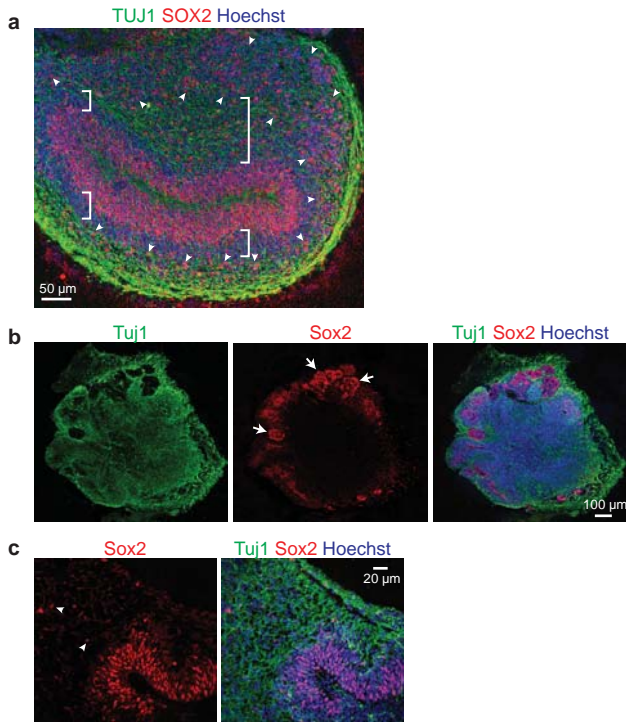
**Extended Data Figure 3 | RG organization and morphology.** **a**, Staining for the chromatin remodelling BAF components BAF53A (also known as ACTL6A) (green, top panels) and BAF53B (also known as ACTL6B) (green, bottom panels) in serial sections of the same tissue showing the neural-progenitor-specific BAF53A expressed in VZ RGs, whereas the neuron-specific BAF53B is expressed in DCX<sup>+</sup> (red) neurons outside the VZ. **b**, Higher magnification image of p-vimentin staining (green) of a dividing radial glia revealing the long basal process typical of radial glial morphology. **c**, Schematic of electroporation technique. Plasmid DNA was injected into fluid-filled cavities within the organoid and an electric pulse was applied to electroporate

cells (radial glial progenitors) adjacent to the cavity. This resulted in several regions of electroporation (top right, GFP in green) and high efficiency of electroporation of RGs (bottom, GFP in green). **d**, GFP-electroporated progenitors (arrows) in an early stage tissue (18 days) revealing neuroepithelial morphology. **e**, GFP-electroporated tissue at 30 days, revealing RG (arrows) with typical bipolar morphology (arrowheads). **f**, GFP-electroporated tissue at 36 days revealing more advanced thicker cortical region with RG (arrow) exhibiting long apical and basal processes (arrowheads). **g**, p-Vimentin (green) staining revealing a mitotic cell at the apical surface during anaphase (arrow) with a horizontal orientation of division.

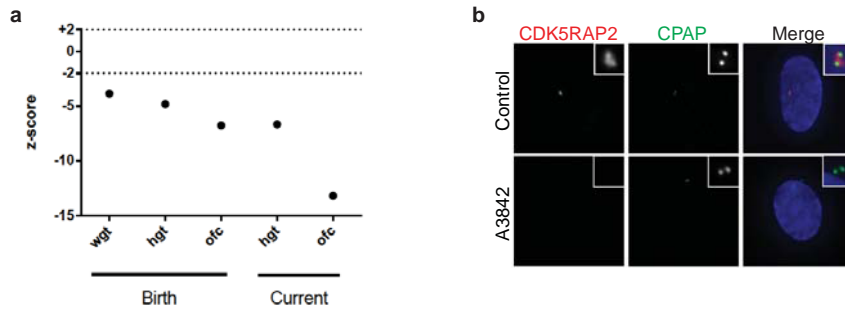


**Extended Data Figure 4 | Spatial organization and characteristics of cortical neuron identities.** **a**, Staining for the preplate marker TBR1 (green) and the deep-layer marker CTIP2 (red) at day 30, revealing rudimentary spatial separation reminiscent of the early stages of cortical plate development. **b**, Immunohistochemistry for the early-born neuron marker CTIP2 (green) and later-born neuron marker BRN2 (red) reveals independent neuron populations exhibiting rudimentary separation at 30 days of differentiation.

**c**, GFP (green)-electroporated neuronal axon 5 days after electroporation displaying complex morphology and axon branching (arrowheads). **d**, GFP (green)-electroporated cortical neurons (arrows) 5 days after electroporation extend long-range axons with evidence of axon bundling (arrowheads) similar to that seen in pyramidal tracts. **e**, Single-cell tracings of calcium surges in individual neurons (ROI, outlined in left panel) as measured by change in fluorescence (arbitrary units).

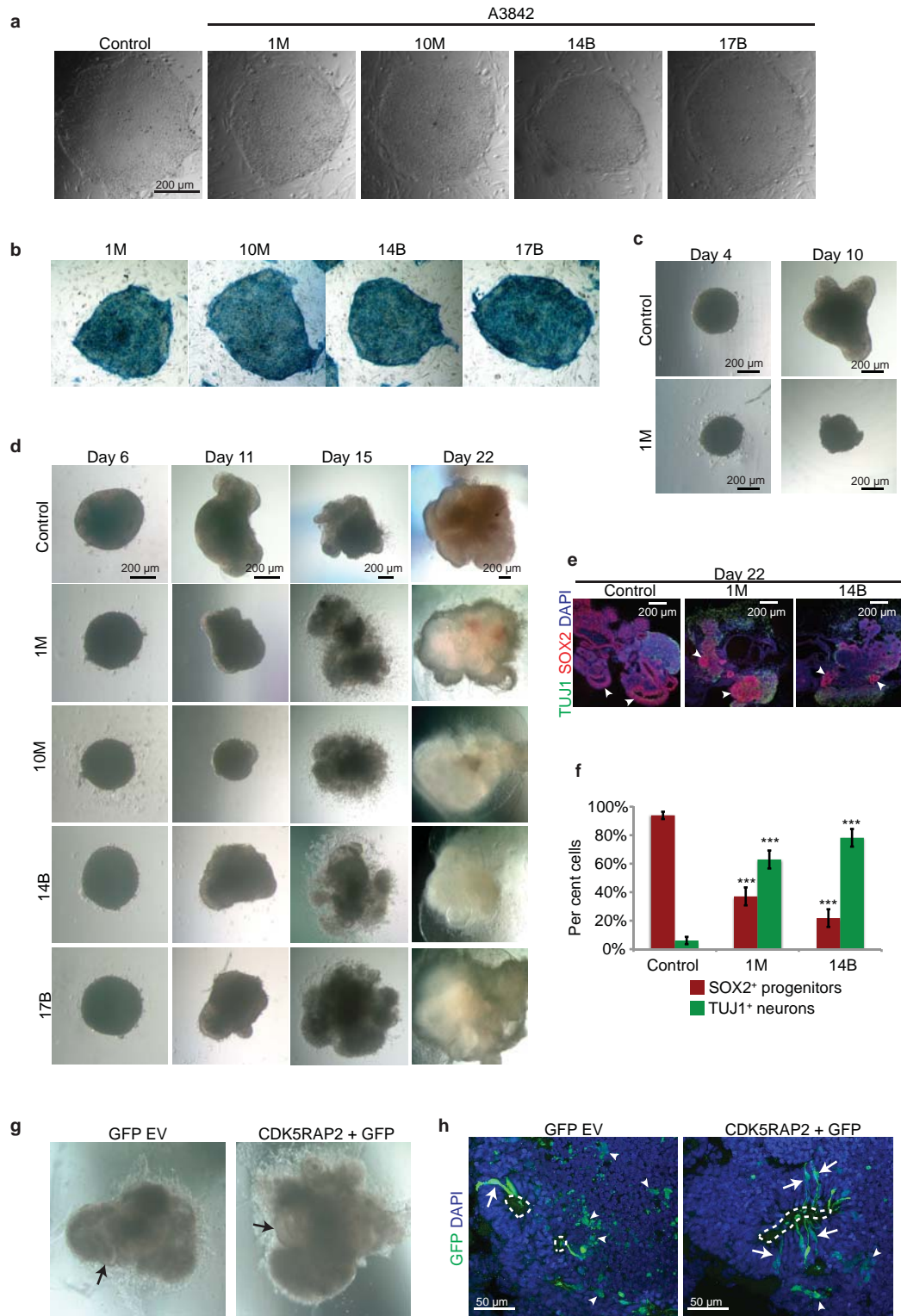


**Extended Data Figure 5 | Human features of cortical development are not recapitulated in mouse organoids.** **a**, Low-magnification image of the region shown in Fig. 5a revealing the presence of a separated region of oRGs (demarcated by arrowheads) that appear separate from the VZ in all regions (brackets) but more separated and with a layer of TUJ1<sup>+</sup> fibres in between in thicker parts of the cortical tissue (larger bracket). The entire organoid can be seen in Fig. 1c. **b**, Low-magnification image of a cerebral organoid derived from mouse ES cells stained for neurons (Tuj1, green) and neural progenitors (Sox2, red) revealing overall smaller organoid size as well as smaller cortical regions (arrows) than in humans. **c**, Higher magnification of a region of cortical identity in mouse cerebral organoids stained for RG progenitors (Sox2, red) revealing the presence of only a few oRGs (arrowheads) that do not organize into a separate layer such as that seen in humans.



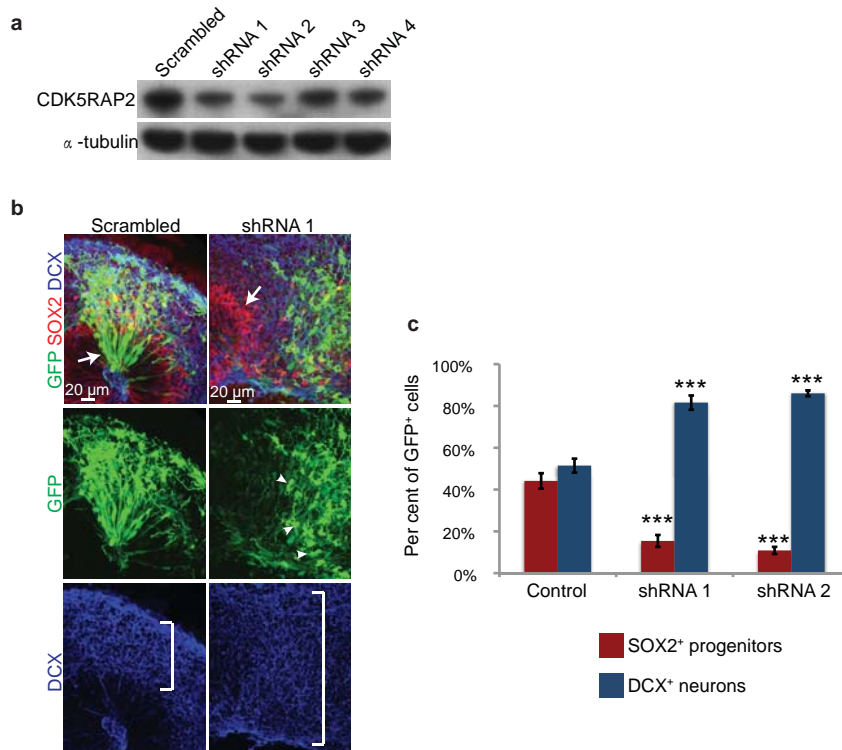
**Extended Data Figure 6 | Patient growth parameters.** **a**, All growth parameters were significantly reduced both at birth and postnatally, with all z-scores less than  $-2$  s.d. from the population mean for age and sex (dashed line). Weight (wgt), height (hgt) and head circumference (occipitofrontal circumference, ofc) at birth and at current age of 3.5 years of age. Head

circumference was much more severely affected than height and weight, indicating that brain volume was disproportionately reduced as a result of more severe growth restriction. **b**, CDK5RAP2 (red) is absent from the centrosome in patient fibroblasts. Immunofluorescent microscopy images of patient (A3842) and control cells, also stained with the centriolar marker CPAP (green).



**Extended Data Figure 7 | Characterization of patient-derived iPS cells and cerebral organoids.** **a**, iPS cells derived from A3842 patient skin fibroblasts exhibit typical ES-cell-like morphology. Four lines were chosen for analysis on the basis of this typical morphology and pluripotency. **b**, Alkaline phosphatase staining (blue) of patient-derived iPS cell colonies revealing pluripotency. **c**, Representative early organoid culture of patient (line 1M) and control using the protocol and timing established for normal human ES cells. Patient organoids were much smaller and failed to thrive, therefore the protocol was slightly modified with increased starting cell number to produce neural tissues. **d**, Patient-derived tissues using increased starting cell number displayed neuroepithelium but did not form thick fluid-filled cortical tissues compared with control-derived tissues. Patient-derived tissues also display outgrowth with neural morphology compared with control. **e**, Staining of patient and control organoids at an early stage (day 22) for neurons (TUJ1, green) and RG

(SOX2, red) revealed smaller progenitor zones (arrowheads) and increased neurons in patient-derived tissues (lines 1M and 14B are shown here). **f**, Quantification of the percentage of SOX2<sup>+</sup> progenitors and TUJ1<sup>+</sup> neurons in cerebral cortical regions of control and two lines of patient-derived tissues (1M and 14B) at the early stage of day 22. Error bars are  $\pm$  s.e.m. \*\*\* $P < 0.001$  compared with control, Student's *t*-test.  $n = 4$  tissues for each line. **g**, Bright-field image of patient-derived tissues (line 14B) electroporated with either GFP alone (left panel) or a GFP and CDK5RAP2 expression construct (right panel). Note the presence of larger neuroepithelial tissue (arrows) in CDK5RAP2-electroporated tissue compared with control. **h**, GFP staining (green) in GFP control (left) and CDK5RAP2 co-electroporated patient-derived tissues (14B) revealing the presence of multiple GFP<sup>+</sup> neurons (arrowheads) in control 6 days after electroporation, whereas CDK5RAP2-electroporated tissues display multiple GFP<sup>+</sup> RG (arrows).



**Extended Data Figure 8 | shRNA-mediated knockdown of *CDK5RAP2* in human organoids.** **a**, Western blot for endogenous *CDK5RAP2* in 293T cells transfected with four different shRNAs against *CDK5RAP2*. shRNAs 1 and 2 are most efficient, whereas shRNA 4 leads to a modest reduction in protein.  $\alpha$ -Tubulin is shown as a loading control. **b**, Higher magnification of results in Fig. 6i showing neuronal morphology of *CDK5RAP2* shRNA (GFP, green, arrowheads)-electroporated cells. These exhibit increased DCX (blue)

expression with an expansion of the zone of DCX positivity (bars) and a loss of SOX2 (red) compared with scrambled electroporated or adjacent non-electroporated tissue (arrows). **c**, Quantification of the percentage of GFP<sup>+</sup> electroporated cells exhibiting SOX2<sup>+</sup> progenitor identity or DCX<sup>+</sup> neuronal identity in scrambled control- or shRNA-co-electroporated tissues. \*\*\* $P < 0.001$  compared to control, Student's *t*-test,  $n = 4$  tissues for each shRNA. Error bars are  $\pm$  s.e.m.